Int. J. Electrochem. Sci., 14 **(2019)** 11312 – 11324, doi: 10.20964/2019.12.69

International Journal of
ELECTROCHEMICAL
SCIENCE
www.electrochemsci.org

Effects of Ultrasound on the Microstructure and Corrosion Behaviour of a PEO Coating

Guo-rui Wu[1,2], *Dong-dong Wang*[1], *Xin-tong Liu*[1], *Yan Wang*[1], *Dong Chen*[1], *Mingjia Wang*[1], *Dejiu Shen*[1,*]

[1] State Key Laboratory of Metastable Materials Science and Technology, College of Materials Science and Engineering, Yanshan University, Qinhuangdao 066004, PR. China
[2] CITIC Dicastal Limited by Share Ltd, Qinhuangdao 066000, PR. China
[*]E-mail: DejiuShen@163.com

Received: 2 August 2019 / *Accepted:* 22 September 2019 / *Published:* 29 October 2019

The plasma Plasma electrolytic oxidation (PEO) coatings were prepared on pure aluminium with and without the assistance application of ultrasound, respectively. The effect of ultrasound on the coating microstructure, chemical and phase compositions, and on the corrosion resistance were investigated by means of using a the scanning electron microscope (SEM) equipped with an energy dispersive spectrometry (EDS), an X-ray diffractomerter (XRD), potentiodynamic polarization and electrochemical impedance spectroscopy (EIS). The results showed that ultrasound could advance the dielectric breakdown time of the PEO coating, and homogenize the coating structure and the distributeion of Si elements in the coatings without affecting the phase composition. The corrosion resistance of the PEO coating was also improved by ultrasound.

Keywords: plasma electrolytic oxidation; ultrasound; corrosion resistance

1. INTRODUCTION

Plasma electrolytic oxidation (PEO) is a surface treatment process which that can generate a metallurgical ceramic-like coating on the surface of valve metals or their alloys [1-6]. PEO is considered to be a very promising technology due to the its environmentally friendly preparation method, along with providing strong coating-substrate bonding, and the excellent corrosion and abrasion resistance and large specific surface area of the resultant coating. PEO coatings have been applied in aerospace, and automotive engineering, along with textiles industry, biomedical devices, and optical function materials [7].

Plasma discharge is considered as an important role in the coating growth, which can melt and oxidize the coating and substrate and forced the melt to erupt, exposing the which exposes fresh substrate

to the oxidizing atmosphere, which also and promotesd the incorporation of electrolytic elements in electrolytes into the coatings [8]. To change the plasma discharge process and fabricate the a satisfactory coating, deploying adjusting electrolyte compositions and adjusting the treatment parameters are widely used by researchers [9-14]. Alkaline aluminates, phosphates and silicates solutions are usually chosen as the basic electrolytes of the PEO process. In the case of the alkaline silicates electrolytes, the prepared coating prepared in the alkaline sodium silicate electrolyte had a large thickness, superior surface roughness and wettability characteristics [15]. However, the long-term PEO process easily formed a large amount of the mullite phase, which often gathered around discharge channels;, the above behaviour increaseding the coating surface roughness of the coating and deteriorateding the coating hardness [16, 17].

Based on the vibration and cavitation effects of ultrasounds, the ultrasound technology has been widely used for a wide range of application in the field of the material preparations, medical exploration, and engineering. Ultrasound has been used as an auxiliary measure in the electroless plating, and electrochemical plating and melts solidifying melt solidification to improve the homogeneity of cladding materials and refine the grains of solidification materials [18-20]. In the previous work, ultrasound was successfully applied in the PEO process of 6061 alloy, and the results indicated that ultrasound could reduce the dielectric breakdown voltage of the coating and increase the coating growth rate [21].

In this work, the effect of ultrasound on the morphology, chemical and phase composition and along with the corrosion resistance of the coating prepared on pure Al under a constant current density regime had been was investigated. Electrochemical impedance spectroscopy (EIS) and a patented electrochemical detachment technique were used to estimate the microstructure, homogeneity and corrosion behaviour of the coating.

2. EXPERIMENTAL

AA1060 pure aluminium (0.05% Cu, 0.05% Mg, 0.03% Mn, 0.05% Zn, 0.03% Ti, 0.25% Si, 0.35% Fe and Al balance) samples with a dimensions of 15 mm × 15 mm × 0.2 mm were ground by 3000 grit sandpapers and ultrasonically cleaneding with acetone, progressively. The electrolyte was prepared by 8 g/L sodium silicate and 2 g/L sodium hydroxide in deionized water. The samples were fabricated PEO-coated using a self-made experimental setup homemade equipment with an asymmetric AC power supply under a constant current density of 4.4 A/dm^2 regime. During the PEO process, the voltages were recorded by a USB4702 data acquisition system with a sampling time of 1 ms controlled by NI Labview software. The temperature of the electrolyte was kept below 30 ± 2°C by a cooling system during the PEO process. The power and frequency of the ultrasonic vibration device were 100 W and 35 kHz, respectively. The parameters of the ultrasonic vibration device used in this work were set as follows: frequency, 35 kHz and power, 100 W. After the PEO process, the PEO coated samples were thoroughly rinsed with deionized water and then dried by air flow. The typical PEO treatment times were set at as 1 min, 4 min, 16 min and 30 min, and the corresponding PEO coated samples fabricated by the ultrasound-assisted PEO process (UAP) were named as U-1, U-4, U-16 and U-30, respectively; the PEO coated samples fabricated by traditional PEO process (TP) were named as T-1, T-4, T-16 and T-30,

respectively. After the PEO process, some coatings were detached from substrates by an electrochemical detachment technique which has been detailedly described in detail in our previous work [22].

A COOLPIX Nikon video camera with an 800 K pixel CCD, a 40x optical zoom and a 40 mm lens filter was used to record the real-time spark images during the PEO process were captured using a coolpi Nikon video camera (800 K pixels CCD, 40× optical zoom and 40 mm lens filter). The surface morphology, and the cross-sectional and elemental composition of the PEO coatings were evaluated by a scanning electron microscope (SEM, Hitachi S-4800, Japan) in the secondary electron (SE) mode and the with energy dispersive spectrometer (EDS). The phase composition of the PEO coatings was investigated using an by the X-ray diffractometer (XRD, D/MAX-rB) with Cu Kα radiation at 40 kV and 100 mA at a scanning rate of 2°/min over the 2θ range of 10° and 80°.

The corrosion behaviour of the PEO coating was characterized by the potentiodynamic polarization and electrochemical impedance spectroscopy (EIS) tests using the RST5000 electrochemical workstation corrosion test system in a 0.1 M NaCl aqueous solution at room temperature. A conventional three-electrode system with a saturated calomel electrode (SCE) as a reference electrode , a counter electrode of platinum foil and a working electrode was used, in which the working electrode was a PEO-coated sample with an area of 1 cm^2 exposed to the solution. cell was used, which was composed of a saturated calomel electrode (SCE) as the reference electrode, a platinum foil as the counter electrode, and a PEO-coated sample with an exposed area of 1 cm^2 to the solution as the working electrode. The scanning rate of potentiodynamic polarization tests scanning was conducted at a rate of 1 mV/s. The EIS was recorded in the frequency range of 0.01 Hz - 100 kHz and with an the amplitude voltage of 5 mV versus OCP, and analysed by fitting to an appropriate electrical equivalent circuit using ZSimpwin software.

3. RESULTS AND DISCUSSION

3.1 Voltage–time responses and spark progression of the PEO process

The voltage-time responses during the UAP and TP processes are shown in Fig. 1, as well as the spark progression pictures. From Fig. 1, it can be seen that for both conditions, the voltage increases at a fast rate in the beginning, and slows down around reaching the at approximately 400 V.

This turning point is considered as to be the dielectric breakdown of the coatings [23]. After which Then, the voltage increases at a much slower pace. Evidently, the ultrasound advanced the time of dielectric breakdown, furthermore, it can also be seen that throughout the entire PEO process, the voltage during the PEO process is notably higher when ultrasound was implemented. Also Additionally, from the spark progression pictures, it can be observed that the sparks start from small and closely packed white sparks and gradually grow to bigger large, and orange-yellow sparks. When the processing time was 5 s, small micro-discharges could can be found on the sample surface in the UAP process. However, not until the a processing time of extended to 20 s did, similar micro-discharges just appeared on the sample surface in the TP process, which is consistent with the information indicated by the voltage-time responses. A possible explanation may be that the cavitation effect of ultrasound promoted the

circulation of the electrolyte and reduced the solution resistance. Furthermore, the mechanical vibration of the ultrasound can also can let allow the breakdown voltage more easily to be reached more easily by increasing the temperature at the coating/electrolyte interface and fabricating micro flaw in the newly formed coating [21].

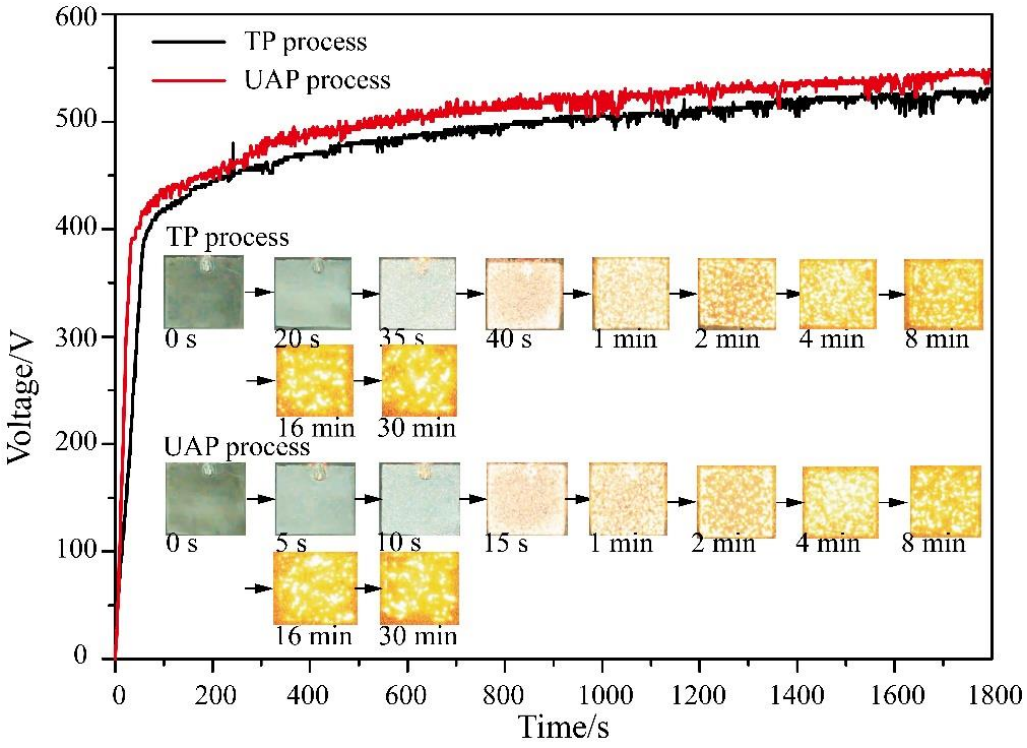

Figure 1. Voltage–time responses during the UAP and TP processes and the related spark progression pictures.

3.2 Microstructures and compositions

The surface morphologies of the PEO coatings fabricated in UAP and TP processes are shown in Fig. 2. It can be seen that there are many micro crater structures on PEO coating surfaces, which should be caused by the evolution of gasses or eruption of melts during discharges [24]. Before the initial 4 min, there seemed to be more pores on the coating surfaces formed by the UAP process seemed more than that the number formed by the TP process, which should be related to the ultrasound increasinged the number of discharges. Other studies have suggested that the energy of ultrasound can transform into thermal energy when the wave reaches the coating/electrolyte interface, which promotes the dissolution of the existing coating at some local regions, thus forming weaker regions and allowing more discharges to be established [21]. Over the next 12 min of the process period, these crater structures were transformed into pancake structures surrounded by numerous nodules. In fact, this nodule structure is a silicon-rich phase and that is most likely mullite [4].

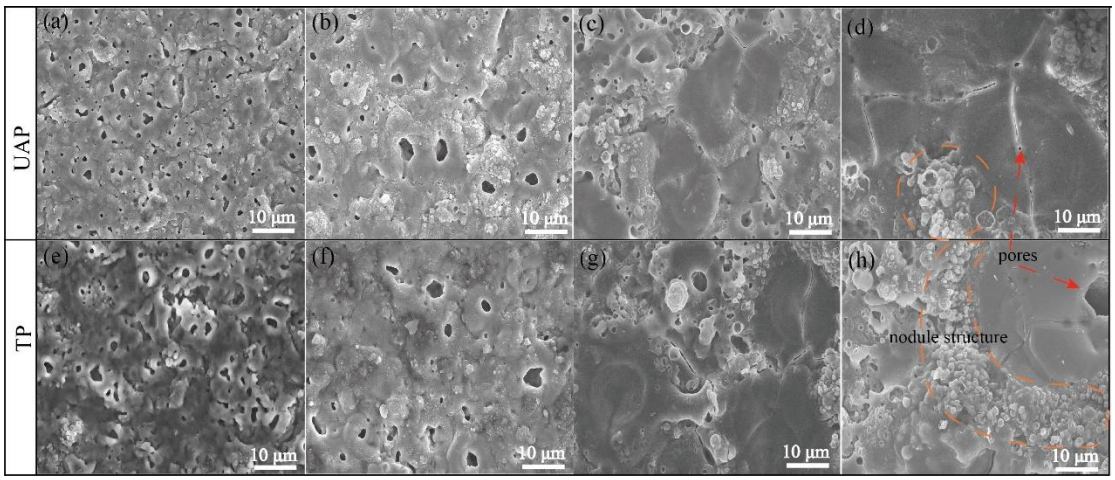

Figure 2. Surface morphology of PEO coatings obtained in the UAP and TP processes: (a) U-1, (b) U-4, (c) U-16, (d) U-30, (e) T-1, (f) T-4, (g) T-16 and (h) T-30.

During the final 14 min, these pancake structures were twice as large as those formed in the previous period. Notably, the surface of U-30 appeared smoother than that of the T-30 because of the reduction of decrease in nodule structures. In addition, the pores in the U-30 coating were much smaller in number and size than those in the T-30 coating, which should be affected by the vibration and cavitation of ultrasound. PEO coatings were melted by the high temperature generated by discharge activities, and the melts would be were pressed out of the coating under the joint effects of the melt vapor pressure and ultrasound vibration, while the cavitation of ultrasound would force melts to crawl on the coating surface or even back to the discharge channels., As a result, a smoother coating surface with small pores was obtained on the with sample U-30.

Fig. 3 shows the cross-sections of the pure coatings obtained by the UAP and TP processes. As shown in Fig. 3 (a) and (b), all coatings obtained by UAP and TP processes had a dual-layer structure, which included a compact inner barrier layer and a porous outer layer, and some differently-sized cavities with different sizes between them. The structures of the coatings varied with the PEO treatment time and applied conditions (UAP and TP). As shown in Fig .3 (a) and (e), under the effect of ultrasonic ultrasound, the cavity and discharge channel in coating U-1 was smaller than the one that in coating T-1, which is in line with the surface morphology. It is well known that under the same electrical parameter, the increase in the number of discharges will reduce the intensity of a single discharge, and the size of the resulting discharge channels and cavities will also decrease. Therefore, these changes are due to the effects of the ultrasound and causes an increasing discharge number while decreasing their average size [21, 25]. When prolonging the treatment time to 4 min, the coating thickness of U-4 exceeded that of the coating of T-4, indicating that the ultrasound accelerated the coating growth rate. As shown in Fig. 3 (c), the outer layer of U-16 was a relatively smooth structure, while that of T-16, however, seemed unsmooth rough and nonuniform, which may be caused by the compression effect provided by the ultrasound [26]. During discharges, melts are ejected from the inside coating and smeared on the coating surface. At this time, the compacting force imparted by the ultrasound compels these incompletely solidified melts to spread more evenly; as a result, a more homogenized coating is formed. Furthermore, the coating of U-30 still clearly remained the clearly in the dual-layer structure, while the outer and inner barrier layers

of the T-30 were not clearly differentiated, and the along with numerous pores having been distributed in the coating of T-30.

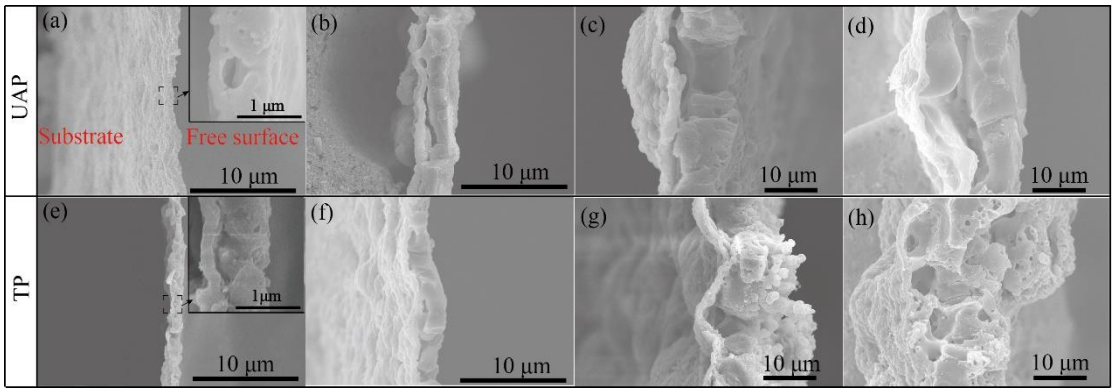

Figure 3. Cross-sections of pure PEO coatings obtained in the UAP and TP processes: (a) U-1, (b) U-4, (c) U-16, (d) U-30, (e) T-1, (f) T-4, (g) T-16 and (h) T-30.

In order to To study the elemental distribution in the coating, the PEO-coated samples (U-30 and T-30) were inlaid and polished, and the concerned examined cross-sections are shown in Fig. 4. It The result suggested that the coatings obtained under both conditions formed a strong metallurgical bond with the substrate. However, since the pores inside the coatings were filled with resin during the inlay process, the cross-sections of the coatings could not show the micro details as the above pure coating (Fig. 3). As shown by the elemental distribution, the distributions of Al and O elements were rather even in the U-30 and T-30 coatings, and there were some Si elements distributed at the coating surface. However, for the U-30 coating, besides in addition to the Si elements on the coating surface, there were some Si elements in the inner layer, indicating that the ultrasound promoted the diffusion of Si elements to the coating inside and improved its segregation state. With the increase of the coating thickness, the Si elements from the electrolyte became harder to transfer towards the substrate through the discharge channels, causing the Si element content in the inner barrier layer to be less. and Instead the Si gathered at the coating surface and formed into some Si-rich phases. However, the mechanical vibration of the ultrasound accelerated the electrolyte circulation and promoted the reaction of the electrolyte with fresh substrate. Accelerating electrolyte circulation by ultrasound is confirmed in other work [21]. Therefore, the inner layer of U-30 containeds a larger amount of Si elements than that of T-30, and U-30 had a smoother coating surface (see Fig. 2).

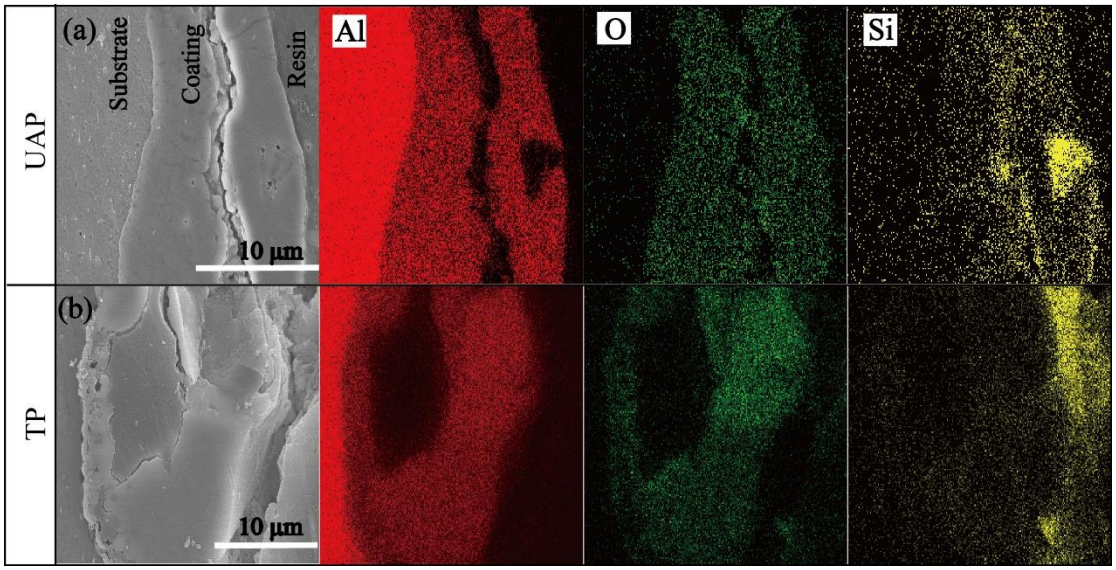

Figure 4. Cross-sections and related element distribution of the samples with substrates, (a) U-30 and (b) T-30.

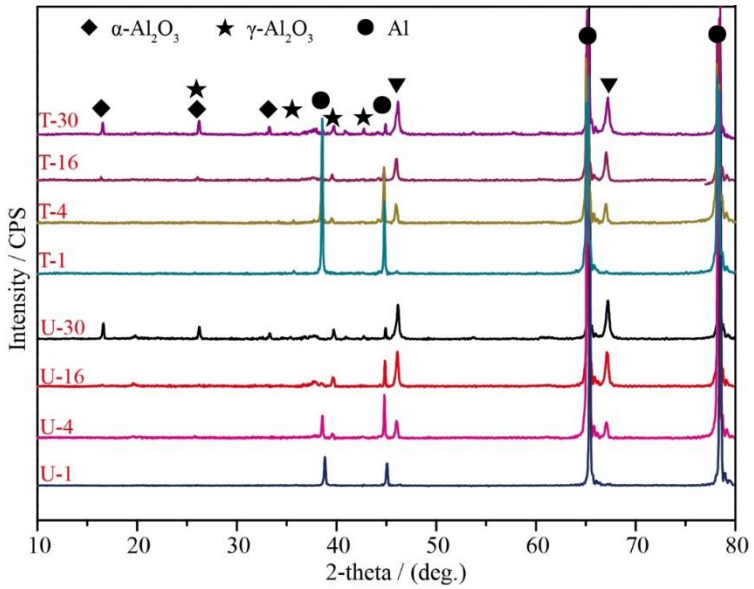

Figure 5. XRD patterns of PEO coatings obtained in the UAP and TP processes.

Fig. 5 shows the XRD patterns of the PEO coatings formed at different times under the two conditions. The results showed that at the early stage of the PEO process, the coating compositions (U-1, U-4, T-1 and T-4) were mainly γ-Al_2O_3 and α-Al_2O_3 phases. When the PEO process reached the mid to late stage, the compositions changed to be a mixture of γ-Al_2O_3, α-Al_2O_3 and mullite phases. Moreover, the result also indicated that the coating phase composition was not affected by the ultrasound, which may be due to the low power and frequency of the ultrasound applied in this work (100 W and 35 kHZ, significantly lower than that 500 W [21] or 130 kHz [25] in other work). The low power and

frequency oscillation of the ultrasound is not sufficient to provide the required energy for lattice distortion during the transition process of γ-Al_2O_3 to α-Al_2O_3.

3.3 Corrosion resistance tests

3.3.1 Potentiodynamic polarization tests

Fig. 6 shows the polarization curves of the AA1060 substrate as well as the individual potentiodynamic polarization curves of the PEO coated samples produced by the UAP and TP processes at different times. The related electrochemical parameters of corrosive current density (i_{corr}), the corrosive potential (E_{corr}) and polarized resistance (R_p) were calculated from the polarization curves and listed in Table 1, where R_p was calculated using the Stern Geary formula [27].

$$R_p = \frac{b_a \times b_c}{2.303 i_{corr}(b_a + b_c)} \quad (1)$$

As shown in Fig. 6, the overall i_{corr}s of the PEO coated samples produced by UAP and TP processes were smaller than that of the bare substrate, indicating that PEO treatment could significantly improve the corrosion resistance of the substrate.

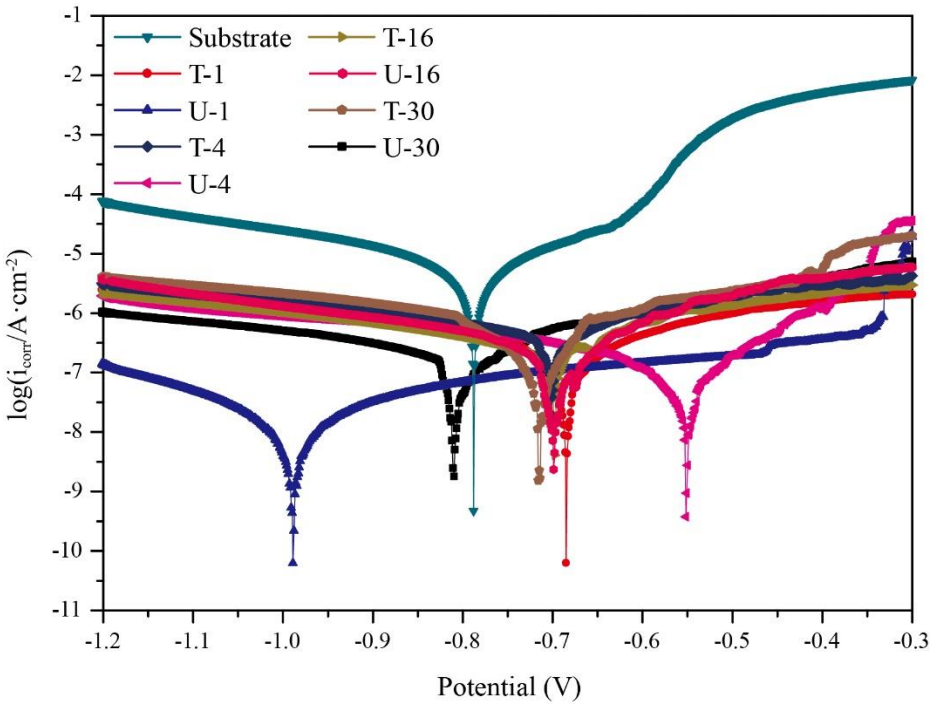

Figure 6. Potentiodynamic polarization curves of the substrate and the PEO coatings obtained in the UAP and TP processes.

Furthermore, the lowest corrosion current densities of the coatings obtained in the UAP and TP processes were achieved at U-1 and T-1, respectively. With increasing extending the PEO treatment time, the corrosion current density gradually increased gradually, indicating that the corrosion resistance of the coating was gradually deteriorated., which The above behaviour should be caused by the

increasing number of pores on the PEO coating. However, at the same treatment duration, the corrosion resistance of the coating obtained by the UAP process was considerably larger than that of the coating obtained by the TP process, which suggested that the assisted assistance from the ultrasound could optimize the corrosion resistance of the PEO coating to some extent.

Table 1. Potentiodynamic corrosion data in 3.5 wt.% 1 M NaCl solution for the substrate and PEO coated samples obtained in the UAP and TP processes.

Samples	E_{corr}(V)	i_{corr}($\times10^{-8}$A/cm^2)	b_a(mV/dec)	b_c(mV/dec)	R_{corr}($\times10^5\Omega\cdot$cm^2)
Substrate	-0.785	391	158	183	0.944
U-1	-0.995	0.978	168	151	355
T-1	-0.704	5.62	379	115	68.6
U-4	-0.551	7.93	120	168	38.4
T-4	-0.709	11.5	122	227	30.0
U-16	-0.689	14.2	175	181	27.1
T-16	-0.702	15.5	151	298	28.0
U-30	-0.810	28.2	160	289	19.2
T-30	-0.710	32.7	194	382	17.1

3.3.2 EIS tests

The corrosion behaviour of the bare substrate and the PEO coatings obtained with in different treatment durations by of the UAP and TP processes were evaluated by EIS tests., Nyquist (complex plane) and Bode diagrams are shown in Fig. 7. According to the Bode-phase plots, the spectra showed two time constants for all PEO-coated samples produced in the different treatment durations by of the UAP and TP processes, indicating that the coatings had a dual-layer structure; which this observation was in accordance with the results provided by the cross-sections. The Bode-impedance plots showed that at low frequency (0.01 Hz), the impedance value of U-1 was the largest one among all samples, and the impedance of the bare substrate was the smallest one, which was in agreement with the results suggested by the potentiodynamic polarization tests. The Nyquist plots of the PEO-coated samples consisted of a small capacitive loop at high frequencies and a large capacitive loop at low frequencies, which were corresponding corresponded to the porous outer layer and the compact inner barrier layer of the PEO coatings, respectively.

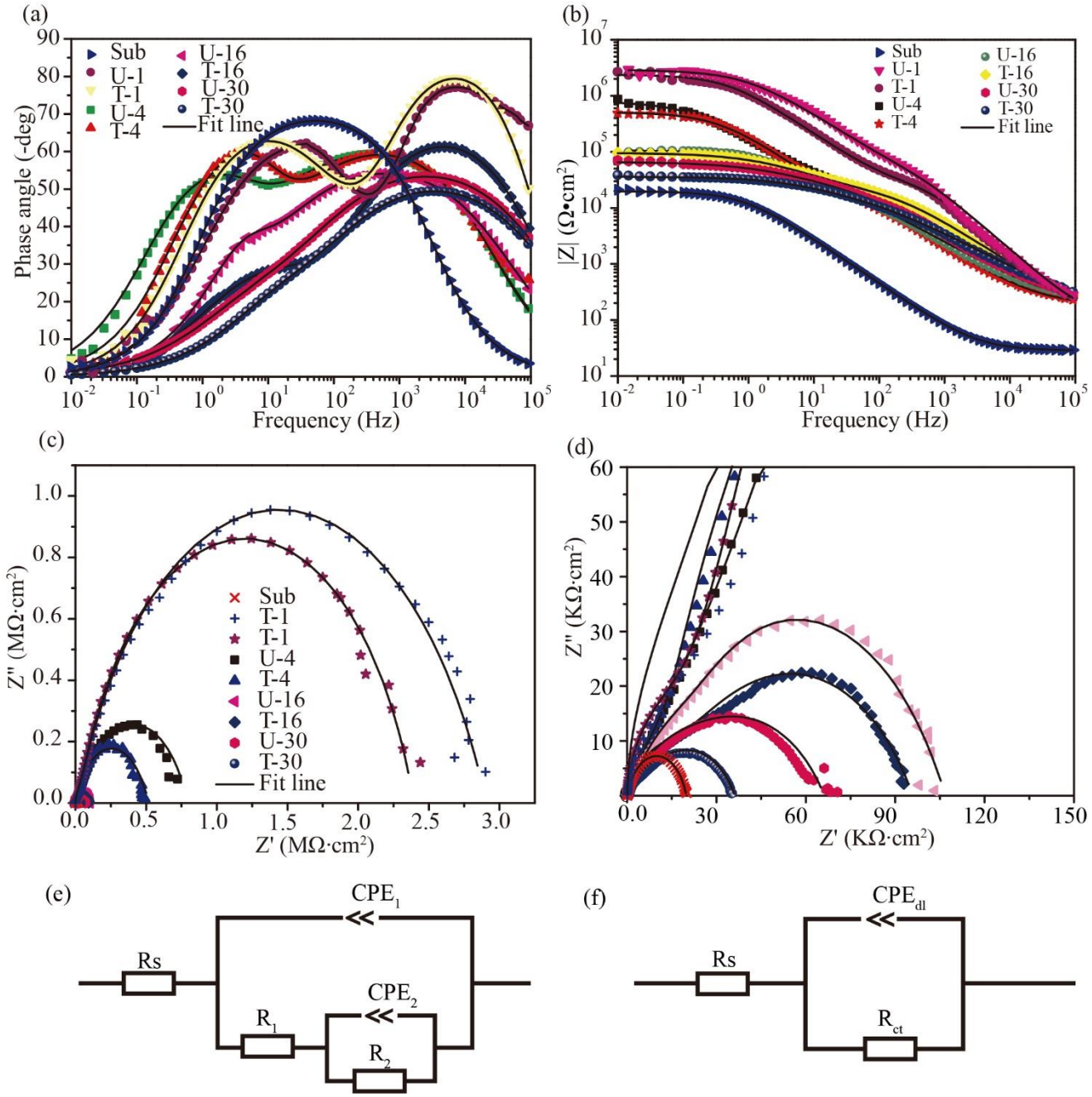

Figure 7. EIS and corresponding equivalent circuits of the PEO coatings obtained by the UAP and TP processes: (a) Bode–phase plots, (b) Bode–impedance plots, (c) Nyquist plots, (d) magnified plots of (c), (e) equivalent circuit of the PEO coatings, and (f) equivalent circuit of the bare substrate.

For quantitative analysis, the EIS data were simulated by the ZSimpwin software using the corresponding equivalent circuits, $R_s(CPE_{dl}R_{ct})$ and $R_s(CPE_1(R_1(CPE_2R_2)))$, for the bare substrate and PEO coatings, as shown in Fig. 7 (e) and (f), respectively. The fitted data of the electrical elements were are listed in Table 2. In the corresponding equivalent circuits, R_s represents the resistance of the solution between the working and reference electrodes, R_1 represents the resistance of the outer layer paralleled with a constant phase element (CPE_1), R_2 represents the resistance of the inner barrier layer paralleled

with a constant phase element (CPE_2), CPE_{dl} represents the double layer capacitance between the electrolyte and the substrate, and R_{ct} represents the charge transfer resistance. The impedance of CPE is determined by the following equation [28]:

$$Z_{CPE} = \frac{1}{Q((j_\omega)^n)} \quad (2)$$

where Q is a the fit parameter, j is the imaginary number, ω is the angular frequency and n is the exponent of the CPE. The value of n is between 0 and 1, which is depending and depends on distributed surface reactivity, surface roughness and porosity, and current and potential distributions on the electrode surface [29-31]. According to the fitting data of the equivalent circuit, the value of R_2 was two orders of magnitude larger than that of R_1, indicating that the contribution of the outer layer to coating corrosion resistance was less than that of the inner barrier layer. The largest values of R_1 and R_2 were achieved with the U-1 coating., and with With the prolonging of PEO treatment time, both the values of R_1 and R_2 under the UAP and TP conditions showed a downward decreasing trend, indicating a decreasing corrosion resistance of the outer layer and inner barrier layer.

Table 2. Equivalent component parameters of the aluminium substrate and the PEO coatings obtained in the UAP and TP processes.

Sample	R_s ($\Omega \cdot cm^2$)	R_1 ($\Omega \cdot cm^2$)	CPE_1 ($F \cdot cm^2$)	n_1	R_2 ($\Omega \cdot cm^2$)	CPE_2 ($F\ cm^2$)	n_2
Substrate	30.3	1.36×10^4	1.16×10^{-5}	0.821	-	-	-
U-1	112	7.96×10^4	3.26×10^{-7}	0.794	8.66×10^6	6.33×10^{-6}	0.968
T-1	137	7.53×10^4	4.76×10^{-7}	0.802	6.99×10^6	9.74×10^{-6}	0.981
U-4	140	5.63×10^4	5.89×10^{-7}	0.731	3.31×10^6	2.32×10^{-7}	0.832
T-4	150	5.51×10^4	7.32×10^{-7}	0.655	2.36×10^6	4.23×10^{-7}	0.793
U-16	111	4.95×10^4	7.01×10^{-7}	0.683	1.12×10^6	3.63×10^{-7}	0.610
T-16	122	4.63×10^4	8.32×10^{-7}	0.601	1.01×10^6	6.98×10^{-7}	0.557
U-30	153	3.12×10^4	9.85×10^{-7}	0.867	5.64×10^5	7.99×10^{-7}	0.622
T-30	109	2.99×10^4	9.63×10^{-7}	0.632	5.33×10^5	8.06×10^{-7}	0.593

The value of CPE was is related to the Cl^- absorption content, and a large CPE value generally represents a high amount of adsorption content of Cl^- [32]. As shown by in Table 2, the values of CPE_1 and CPE_2 decreased with extending the increasing PEO treatment duration., indicating The above observation indicated that the Cl^- absorption content of the outer layer and inner barrier layer gradually increased gradually, which may might be suggested a decreasing compactness of the outer layer and inner barrier layer. A high Cl^- adsorption content is more likely to cause the coating to be corroded, and the values of R_1 and R_2, therefore, decreased with prolonging the prolonged PEO treatment time. Moreover, the CPE data of CPE suggested that the CPE_1 and CPE_2 values of the coatings obtained by the UAP processes were generally lower than those of the coatings obtained by the TP processes, implying that the coatings prepared by the UAP process had a more compact outer layer and inner barrier

layer, which may ; the compact layers might indicate a low number of the microcracks and pores in the coating that prepared by the UAP process. As described above, the value of n reflects the surface conditions of the coatings. The n_1 and n_2 values of the coatings obtained by the UAP process, as well as the n_2 values, were larger than those of the coatings obtained by the TP process, indicating that ultrasound could improve the homogeneities of the outer layer and inner barrier layer at during a long PEO process., which The improved homogeneity was also confirmed by the surface morphologies and cross-sections.

Comparing the fitting data of the coatings obtained by UAP and TP processes of at different times, it can be seen that the assisted ultrasound in ultrasound-assisted PEO treatment will slightly increase the values of R_1 and R_2 corresponding to the resistance of the outer and inner barrier layer. It should be related to the effect of the ultrasound on the reduction of the surface roughness and/or porosity of the outer layer (U-30) and the improvement of the coating homogeneity. Therefore, the assisted ultrasound ultrasound-assisted PEO process is beneficial for improving the corrosion resistance and homogeneity of the coating.

4. CONCLUSIONS

Based on the information provided above, several conclusions were drawn as follows:

(1) Ultrasound advanced the dielectric breakdown time of PEO coatings under a constant current density regime.

(2) Ultrasound homogenized the coating outer layer and the inner barrier layer of the coating, and reduces the surface gather of reduced the Si gathered on the surface by facilitating the diffusion of Si to the substrate without affecting the phase compositions of the coating.

(3) PEO coatings significantly improved the corrosion resistance of pure Al, and assisted ultrasound can further improve the corrosion resistance of the PEO coating.

ACKNOWLEDGEMENT

This work was supported by the National Natural Science Foundation of China (Nos. 51671167 and 51171167) and Natural Science Foundation of Hebei Province, China (Nos. A2015203348 and B2015203406).

References

1. E. Matykina, R. Arrabal, P. Skeldon, G. E. Thompson, P. Belenguer, *Surf. Coat. Technol.*, 205(2010) 1668-1678.
2. C. E. Barchiche, D. Veys-Renaux, E. Rocca, *Surf. Coat. Technol.*, 205(2011) 4243-4248.
3. C. Ma, Y. Lu, P. Sun, Y. Yuan, X. Jing, M. Zhang, *Surf. Coat. Technol.*, 206(2011) 287-294.
4. E. Matykina, G. Doucet, F. Monfort, A. Berkani, P. Skeldon, G. E. Thompson, *Electrochim. Acta*, 51(2006) 4709-4715.
5. A. I. Sonova, O. P. Terleeva, *Prot. of Met.*, 44(2011) 65-75.
6. J. J. Zhuang, Y. Q. Guo, N. Xiang, X. Y. Lu, Q. Hu, R. G. Song, *Mater. Sci. Technol.*, 32(2016) 1559-1566.

7. A. E. R. Friedemann, K. Thiel, U. Haßlinger, M. Ritter, T. M. Gesing, S. Plagemann, *Appl. Surf. Sci.*, 443(2018) 467-474.
8. D.-d. Wang, X.-t. Liu, Y.-k. Wu, H.-p. Han, Z. Yang, Y. Su, X.-z. Zhang, G.-r. Wu, D.-j. Shen, *J. Alloy. Compd.*, 798 (2019) 129-143.
9. T. Wei, F. Yan, J. Tian, *J. Alloy. Compd.*, 389(2005) 169-176.
10. Y. Yang, L. Zhou, *J. Mater. Sci. Technol.*, 30(2014) 1251-1254.
11. K. Dong, Y. Song, D. Shan, E.-H. Han, *Surf. Coat. Technol.*, 266(2015) 188-196.
12. A. R. Fatkullin, E. V. Parfenov, A. Yerokhin, D. M. Lazarev, A. Matthews, *Surf. Coat. Technol.*, 284(2015) 427-437.
13. M. Sun, A. Yerokhin, M. Y. Bychkova, D. V. Shtansky, E. A. Levashov, A. Matthews, *Corros. Sci.*, 111(2016) 753-769.
14. A. B. Rogov, A. Yerokhin, A. Matthews, *Langmuir*, 33(2017) 11059-11069.
15. M. Sandhyarani, T. Prasadrao, N. Rameshbabu, *Appl. Surf. Sci.*, 317(2014) 198-209.
16. Y. Cheng, F. Wu, E. Matykina, P. Skeldon, G. E. Thompson, *Corros. Sci.*, 59(2012) 307-315.
17. J. H. Cao, Y. L. Cheng, A. L. Zuo, Z. M. Peng, B. Liang, *Chin. J. Nonferrous Met.*, 24(2014) 934-943.
18. J. Li, T. Momono, Y. Tayu, Y. Fu, *Mate. Lett.*, 62(2008) 4152-4154.
19. X. Jian, H. Xu, T. T. Meek, Q. Han, *Mate. Lett.*, 59(2005) 190-193.
20. F. Touyeras, J. Y. Hihn, X. Bourgoin, B. Jacques, L. Hallez, V. Branger, *Ultrason. Sonochem.*, 12(2005) 13-19.
21. D. Shen, D. He, F. Liu, C. Guo, J. Cai, G. Li, H. Ma, *Ultrasonics*, 54(2014) 1065-1070.
22. C. Liu, D. He, Q. Yan, Z. Huang, P. Liu, D. Li, G. Jiang, H. Ma, P. Nash, D. Shen, *Surf. Coat. Technol.*, 280(2015) 86-91.
23. S. Moon, Y. Jeong, *Corros. Sci.*, 51(2009) 1506-1512.
24. V. Dehnavi, B. L. Luan, D. W. Shoesmith, X. Y. Liu, S. Rohani, *Surf. Coat. Technol.*, 226(2013) 100-107.
25. D. Shen, J. Cai, G. Li, D. He, L. Wu, H. Ma, Y. Xia, C. He, Y. Yang, *vacuum*, 99(2014) 143-148.
26. X.U. Zhiwu, J. Yan, W. Chen, S. Yang, *Mater. Lett.*, 62(2008) 2615-2618.
27. M. Stern, *J. electrochem. Soc.*, 104(1957) 56-63.
28. M. L. Zheludkevich, R. Serra, M. F. Montemor, K. A. Yasakau, I. M. M. Salvado, M. G. S. Ferreira, *Electrochim. Acta*, 51(2005) 208-217.
29. S. V. Gnedenkov, O. A. Khrisanfova, A. G. Zavidnaya, S. L. Sinebryukhov, V. S. Egorkin, M. V. Nistratova, A. Yerokhin, A. Matthews, *Surf. Coat. Technol.*, 204(2010) 2316-2322.
30. X. Zhang, Z. Yao, Z. Jiang, Y. Zhang, X. Liu, *Corros. Sci.*, 53(2011) 2253-2262.
31. D.-D. Wang, X.-T. Liu, Y. Su, Y.-K. Wu, Z. Yang, H.-P. Han, X.-Z. Zhang, G.-R. Wu, D.-J. Shen, *Surf. Eng.*, (2019) (in press) DOI: 10.1080/02670844.2019.1644935
32. D. Chen, R. Wang, Z. Huang, Y. Wu, Y. Zhang, G. Wu, D. Li, C. Guo, G. Jiang, S. Yu, D. Shen, P. Nash, *Appl. Surf. Sci.*, 434(2018) 326-335.